
Toward Relative Positional Encoding in Spiking Transformers

Changze Lv¹ Yansen Wang² Dongqi Han² Yifei Shen² Xiaoqing Zheng¹ Xuanjing Huang¹ Dongsheng Li²

Abstract

Spiking neural networks (SNNs) are bio-inspired networks that model how neurons in the brain communicate through discrete spikes, which have great potential in various tasks due to their energy efficiency and temporal processing capabilities. SNNs with self-attention mechanisms (Spiking Transformers) have recently shown great advancements in various tasks such as sequential modeling and image classifications. However, integrating positional information, which is essential for capturing sequential relationships in data, remains a challenge in Spiking Transformers. In this paper, we introduce an approximate method for relative positional encoding (RPE) in Spiking Transformers, leveraging Gray Code as the foundation for our approach. We provide comprehensive proof of the method’s effectiveness in partially capturing relative positional information for sequential tasks. Additionally, we extend our RPE approach by adapting it to a two-dimensional form suitable for image patch processing. We evaluate the proposed RPE methods on several tasks, including time series forecasting, text classification, and patch-based image classification. Our experimental results demonstrate that the incorporation of RPE significantly enhances performance by effectively capturing relative positional information.

1. Introduction

Spiking Neural Networks (SNNs) (Maass, 1997) are a class of bio-inspired models designed to emulate the communication process of biological neurons, which transmit information through discrete spikes. In contrast to artificial neural networks (ANNs) that operate on continuous values, SNNs

The work was conducted during the internship of Changze Lv (czlv24@m.fudan.edu.cn) at Microsoft Research Asia. ¹School of Computer Science, Fudan University, Shanghai, China ²Microsoft Research Asia, Shanghai, China. Correspondence to: Xiaoqing Zheng <zhengxq@fudan.edu.cn>, Yansen Wang <yansenwang@microsoft.com>, Dongqi Han <dongqi-han@microsoft.com>.

preprint.

process information in the form of spikes occurring at precise moments in time. This discrete event-driven processing enables SNNs to be highly energy-efficient. The temporal characteristics of spikes make SNNs particularly well-suited for tasks involving sequential data or dynamic environments, such as sensory processing (Li et al., 2017a; Fang et al., 2021), patch-based image classification (Zhou et al., 2023b; Yao et al., 2023), time-series forecasting (Lv et al., 2024b; Park et al., 2024), and natural language processing (Zhu et al., 2023; Lv et al., 2023b; Xing et al., 2024).

In ANNs, relative positional encoding (RPE) is often used to encode the positions of input elements (Su et al., 2024), enabling the model to capture the relative relationships between positions within a sequence. While RPE has been shown to enhance performance in language modeling (Su et al., 2024) and image processing (Liu et al., 2021), its direct application to SNNs remains limited due to the unique characteristics of spike-based computation. Current approaches to realize positional encoding (PE) in SNNs either fail to maintain the uniqueness of spike representations for each position (Zhou et al., 2023b; Yao et al., 2024a), or ignore the incorporation of relative positional information (Lv et al., 2024a).

In this paper, we first identify a limitation in the current spiking self-attention (SSA) mechanism (Zhou et al., 2023b), which is suboptimal for measuring the distance (or similarity) between tokens in the query and key matrices. Specifically, the dot product operation fails to effectively differentiate distances when both the query and key are spike matrices. To address this limitation, we propose a new spiking self-attention mechanism based on the Exclusive-NOR (XNOR) operation, which enhances the measurement of query-key similarity by leveraging the Hamming distance (see Section 3.4).

Secondly, we introduce a novel approximate relative positional encoding method for SNNs, based on Gray Code (Gray, 1953) as the foundational encoding scheme. The consistent Hamming distance between Gray Code representations of two position indices differing by 2^n allows for serving as a spiking RPE method and the integration with the XNOR-based SSA mechanism. The binary encoding nature of Gray Code is well-suited to represent relative positions while preserving the spiking dynamics of SNNs,

which is crucial for effectively processing sequential data. Furthermore, we provide a theoretical proof in Appendix A demonstrating the efficacy of Gray Code in partially capturing relative positional information for sequential tasks.

Moreover, we extend our RPE method to the logarithmic form that can be directly integrated into the attention map of XNOR-based spiking self-attention, offering greater efficiency compared to the previous form while maintaining comparable performance. For image patches, we also design a two-dimensional version of our method to capture the relative positional information of both height and width.

To evaluate the effectiveness of our RPE approaches, we apply them to three diverse tasks: time series forecasting, text classification, and patch-based image classification. Our experiments demonstrate that the proposed RPE method enhances the performance of SNNs across all three tasks, allowing the original SNNs to capture and leverage relative relationships between elements in the input sequential data. Moreover, we further conduct an ablation study and positional encoding analysis to validate the inner properties of our proposed RPE method. Based on the analysis, we offer several valuable insights into designing effective positional encoding schemes for SNNs.

We believe that this work contributes a new method for integrating relative positional encoding into SNNs, expanding their potential for a wide range of applications in machine learning and computational neuroscience. To summarize, our contributions are as follows:

- **A Novel RPE Method for SNNs.** Our research represents one of the pioneering efforts to propose a solution to relative positional encoding for spiking neural networks, albeit as an approximation method.
- **Consistent Performance Improvement.** Our proposed method and its extended variants significantly and consistently improve the performance of SNNs across various sequential tasks, including time-series forecasting and text classification.
- **Theoretical Validation and Insightful Analysis.** In addition to experimental evaluations, we provide thorough theoretical proof to validate the effectiveness of our RPE method. Furthermore, we offer an analysis of the underlying properties of RPE, providing valuable insights for future designs of RPE in SNNs.

2. Related Work

In sequential tasks, positional encoding (PE) plays a crucial role in capturing the order of tokens. Traditional absolute positional encoding assigns a fixed position to each token, whereas relative positional encoding (RPE) emphasizes the distance between tokens. RPE allows the model to generalize across different sequence lengths and better capture

relationships between tokens.

Despite its significance, there has been limited research focusing on the role of positional encoding approaches in spiking neural networks. Notably, both Spikformer (Zhou et al., 2023b) and Spike-driven Transformer (Yao et al., 2023; 2024a) incorporate a combination of convolutional layers, batch normalization, and spiking neuron layers to generate “learnable relative positional encodings”. However, we argue that this approach functions more similarly to a spike-element-wise residual connection (Fang et al., 2021) than to a conventional positional encoding module. A robust PE module should offer unique representations for each position, but the spike-position matrices generated by these methods may lead to identical spike representations for different positions.

Lv et al. (2024a) introduced a spiking positional encoding method for SNNs, inspired by central pattern generators (Marder & Bucher, 2001). This method generates periodic positional encoding, ensuring a unique binary spike matrix for each position. However, their approach is based on absolute positional encoding and, thus, does not capture the time-translational invariance property in many sequential modeling problems, which, however, is an important advantage of relative positional encoding methods.

3. Preliminary

3.1. Spiking Neural Networks

The fundamental building block of SNNs is the spiking neuron, such as the leaky integrate-and-fire (LIF) model (Maass, 1997), which is governed by the input current $I(t)$, influencing the membrane potential $U(t)$ and the spike output $S(t)$ at each time step t . The dynamics of the LIF neuron are captured by the following system of equations:

$$U(t) = H(t - \Delta t) + I(t), \quad I(t) = f(\mathbf{x}; \theta), \quad (1)$$

$$H(t) = V_{\text{reset}}S(t) + (1 - S(t))\beta U(t), \quad (2)$$

$$S(t) = \begin{cases} 1, & \text{if } U(t) \geq U_{\text{thr}}, \\ 0, & \text{if } U(t) < U_{\text{thr}}. \end{cases} \quad (3)$$

Here, $I(t)$ represents the spatial input to the LIF neuron at time t , which is computed by the function f using the input vector \mathbf{x} and the learnable parameters θ . The discretization constant Δt controls the time granularity in the LIF model, and $H(t)$ is the temporal output at time step t . The spike $S(t)$ is determined by a Heaviside step function that is activated when the membrane potential $U(t)$ exceeds a threshold U_{thr} . Upon reaching the threshold, the neuron generates a spike, and $H(t)$ resets to V_{reset} . If $U(t)$ does not exceed the threshold, the membrane potential decays to $H(t)$ at a rate determined by β .

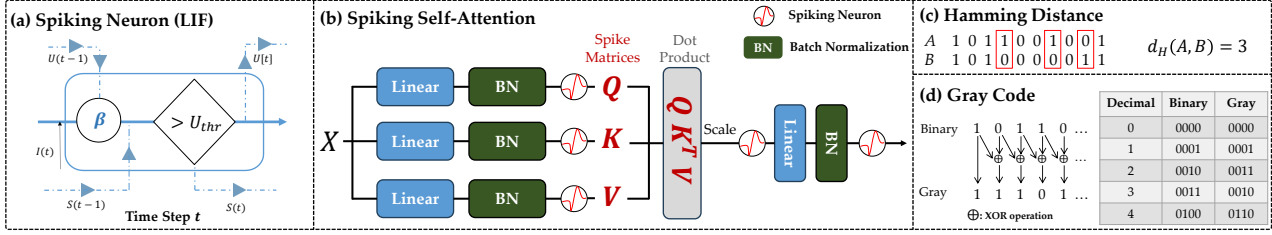


Figure 1. Preliminary Figures. (a) Spike dynamics of spiking (LIF) neurons. (b) Illustration of spiking self-attention in Spikformer (Zhou et al., 2023b) and QKFormer (Zhou et al., 2024). (c) An example of Hamming Distance. (d) Calculation process of Gray Code.

3.2. Spiking Self-Attention

Spiking self-attention (SSA) is a spiking version of self-attention (Vaswani, 2017), which was proposed in Spikformer (Zhou et al., 2023b) and QKFormer (Zhou et al., 2024). The vital design is to utilize discrete spikes to approximate the vanilla self-attention mechanism. It can be written as:

$$\begin{aligned} \mathbf{Q} &= \mathcal{N}(\text{BN}(\mathbf{X} \cdot \mathbf{W}_{\mathbf{Q}})), \\ \mathbf{K} &= \mathcal{N}(\text{BN}(\mathbf{X} \cdot \mathbf{W}_{\mathbf{K}})), \\ \mathbf{V} &= \mathcal{N}(\text{BN}(\mathbf{X} \cdot \mathbf{W}_{\mathbf{V}})), \end{aligned} \quad (4)$$

where \mathcal{N} is a spike neuron layer described in Equation 3. The input is denoted as $\mathbf{X} \in \{0, 1\}^{T \times L \times D}$, where T is the number of time steps. BN represents batch normalization, and τ is a scaling factor. The attention map AttnMap is then computed as the dot product between \mathbf{Q} and \mathbf{K}^T :

$$\text{AttnMap} = \mathbf{Q} \cdot \mathbf{K}^T, \quad (5)$$

$$\text{SSA}(\mathbf{Q}, \mathbf{K}, \mathbf{V}) = \mathcal{N}(\text{BN}((\text{Attn} \cdot \mathbf{V} * \tau) \cdot \mathbf{W})). \quad (6)$$

As a result, the attention map $\text{AttnMap} \in \mathbb{N}_0^{T \times L \times L}$, where \mathbb{N}_0 denotes the set of non-negative integers. The outputs of the SSA, as well as \mathbf{Q} , \mathbf{K} , and \mathbf{V} , are all spike matrices containing only values of 0 and 1. The parameters $\mathbf{W}_{\mathbf{Q}}$, $\mathbf{W}_{\mathbf{K}}$, $\mathbf{W}_{\mathbf{V}}$, and \mathbf{W} are all learnable parameters.

3.3. Relative Positional Encoding

In self-attention mechanisms, the attention weights are modified using a relative positional encoding (RPE) $\mathbf{R}_{i,j}$, which depends on the distance between the i -th and j -th tokens. A typical realization of RPE (Liu et al., 2021; Hao et al., 2024) is formulated as:

$$\begin{aligned} \text{Attention}(\mathbf{Q}, \mathbf{K}, \mathbf{V}) &= \text{AttnMap} \cdot \mathbf{V} \\ &= \text{Softmax} \left(\frac{\mathbf{Q} \cdot \mathbf{K}^T}{\sqrt{d_k}} + \mathbf{R}_{i,j} \right) \mathbf{V}. \end{aligned} \quad (7)$$

Here, $\mathbf{R}_{i,j}$ represents the relative distance between tokens i and j . Specifically, the relative positional encoding for the i -th position in \mathbf{Q} and the j -th position in \mathbf{K} should satisfy **distance consistency**, i.e., the magnitude of $\mathbf{R}_{i,j}$ should depend solely on the relative distance $|i - j|$, enabling the model to distinguish between nearby and distant tokens. This approach improves the model’s ability to handle long-range dependencies and sequence variations.

3.4. Hamming Distance

The Hamming distance between two binary strings of equal length is the number of bit positions at which the corresponding bits are different. Formally, for two binary strings A and B of length m ,

$$d_H(A, B) = \sum_{i=1}^m \delta(A_i, B_i), \quad (8)$$

where

$$\delta(A_i, B_i) = \begin{cases} 1 & \text{if } A_i \neq B_i, \\ 0 & \text{otherwise.} \end{cases} \quad (9)$$

Since the preliminary knowledge involved is extensive and loosely connected, we have provided Figure 1 to help readers visually grasp the key concepts of each section.

4. Method

4.1. Gray Code Definition

Gray Codes (Gray, 1953), also known as reflected binary codes, are binary sequences where consecutive numbers differ by exactly one bit. Gray Code $G(x)$ for a non-negative integer x can be generated using the formula: The standard binary reflected Gray Code $G(x)$ for a non-negative integer x is defined as:

$$G(x) = x \oplus (x \gg 1), \quad (10)$$

where \oplus denotes the bitwise XOR operation, and \gg denotes the arithmetic right shift (with zero padding).

4.2. XNOR-Based Spiking Self-Attention

In the standard self-attention mechanism of Transformer (Vaswani, 2017), the attention map is computed as the dot product between the query matrix \mathbf{Q} and key matrix \mathbf{K} , i.e., $\text{AttnMap} = \mathbf{Q} \cdot \mathbf{K}^T$. The primary concept behind this approach is to use the dot product to measure the **similarity** between each token in \mathbf{Q} and \mathbf{K} , which works effectively when both \mathbf{Q} and \mathbf{K} are continuous-valued matrices. However, when \mathbf{Q} and \mathbf{K} are spike matrices, the dot product becomes inadequate for capturing the temporal or event-based interactions intrinsic to

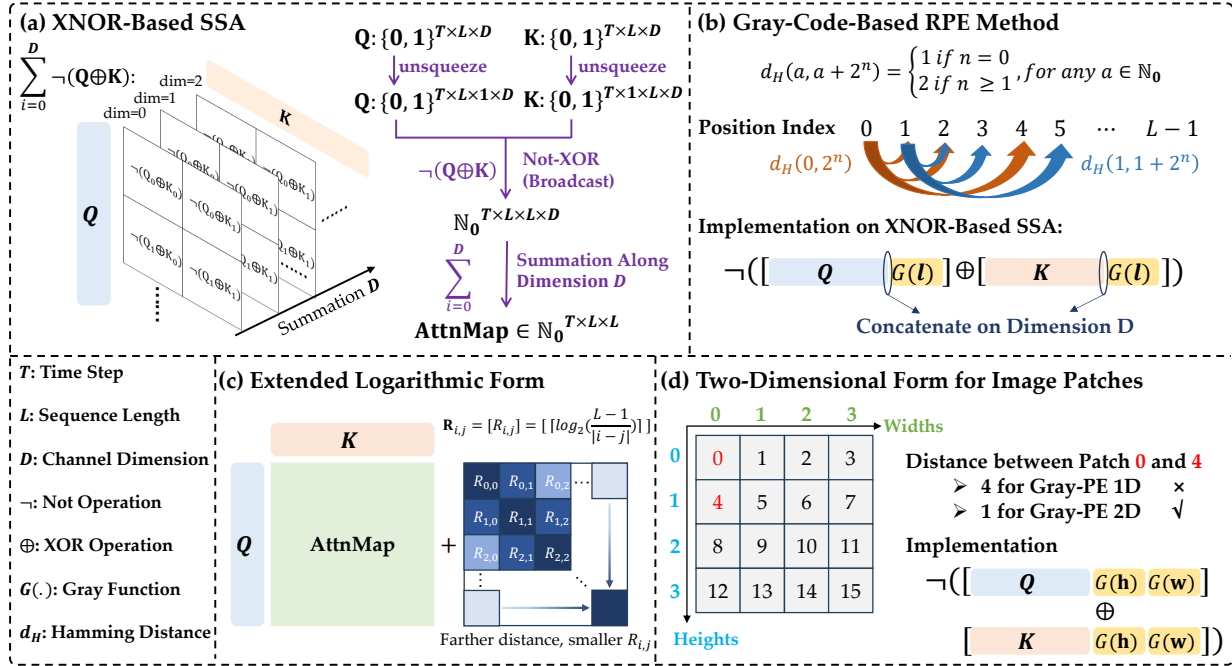


Figure 2. Overview of Our Method. (a) XNOR-based Spiking Self-Attention (SSA). This panel illustrates the computation flow for the query (Q) and key (K) matrices in a PyTorch-style notation. (b) Gray-PE. Gray code representations exhibit a consistent Hamming distance for two integers differing by 2^n . Gray-PE is implemented by concatenating $G(L)$ along the D dimension of both Q and K . (c) Log-PE. A pre-assigned relative distance encoding map $R_{i,j} \in \mathbb{N}_0$ is added to the standard attention map **AttnMap**. The shading indicates the magnitude of the values, with deeper blue corresponding to larger values. (d) 2D Form of Gray-PE. For image patches, a 2D relative positional encoding is more suitable than the 1D version, as it better captures the spatial relationships.

spike-based representations. As a result, the dot product operation in spiking self-attention, as outlined in Section 3.2, is not well-suited for spiking Transformers. To address this limitation, several researchers (Yao et al., 2023; Zhou et al., 2023a; Yao et al., 2024b) have proposed alternative attention mechanisms specifically designed for SNNs.

In this paper, we propose an XNOR-based spiking self-attention mechanism, which leverages the Hamming distance (See Section 3.4) to measure the similarity between each token in Q and K . This approach enables the integration of the Gray-code-based relative positional encoding method into the attention mechanism, allowing for more effective capture of positional information in spike-based representations. Formally, we modify Equation 5 as follows:

$$\text{AttnMap} = \sum_{i=0}^D \neg(Q \oplus K), \quad (11)$$

where \neg denotes the Not operation, \oplus denotes the XOR operation, and D represents the channel dimension. It is important to note that every token in Q will perform XOR \oplus with every token in K , so we sum over the channel dimension D to get **AttnMap** $\in \mathbb{N}_0^{T \times L \times L}$, shown in Figure 2 (a). Compared to the dot product, the XNOR operation significantly increases the values in **AttnMap** $\in \mathbb{N}_0$. Therefore, the scale factor τ in Equation 6 should be set to a smaller

value or treated as a learnable parameter, ensuring that the firing rate of \mathcal{SN} does not become excessively large. We will empirically demonstrate in the Experiments Section that this XNOR modification does not negatively impact the performance of the vanilla spiking self-attention.

4.3. Approximate RPE Method Based on Gray Code

We modify the SSA module by replacing the dot product operation with the XNOR operation, enabling the use of Hamming distance to measure the similarity between tokens. In this context, we propose that Gray Code can serve as an approximate approach to relative positional encoding for SNNs. This is supported by Theorem 4.1, which demonstrates the effectiveness of Gray Code in partially capturing positional relationships within the framework of XNOR-based spiking self-attention.

Theorem 4.1. For two integers differing by 2^n in decimal, their Gray Code representations have a consistent Hamming distance of 1 for $n = 0$, and 2 for $n \geq 1$, i.e., for any non-negative integer a and n :

$$d_H(G(a), G(a + 2^n)) = \begin{cases} 1 & \text{if } n = 0, \\ 2 & \text{if } n \geq 1. \end{cases} \quad (12)$$

Proof. Please refer to Appendix A for detailed proof. \square

From Theorem 4.1, we can infer that Gray Code ensures the consistency of distance representations for every 2^n ($n \geq 0$) relative distance. This property makes Gray Code an ideal approximate RPE method for SNNs, as it not only partially captures relative positions but also preserves the binary nature (0 and 1) nature of SNNs.

In our implementation, we concatenate the Gray Code representations of each position index to both the query matrix $\mathbf{Q} \in \mathbb{N}_0^{T \times L \times D}$ and key matrix $\mathbf{K} \in \mathbb{N}_0^{T \times L \times D}$, leaving the remaining operations unchanged. Formally, the attention map **AttnMap** is computed as follows:

$$\mathbf{AttnMap} = \sum_{i=0}^D \neg([\mathbf{Q} \parallel G(\mathbf{l})] \oplus [\mathbf{K} \parallel G(\mathbf{l})]), \quad (13)$$

where $G(\cdot)$ represents the function that converts non-negative integers into their corresponding Gray Code representations. The vector \mathbf{l} denotes an array of position indexes, specifically $[0, 1, 2, \dots, L-1]$, where L is the sequence length of both \mathbf{Q} and \mathbf{K} . \parallel denotes concatenation on the channel dimension D . We name this method as Gray-PE.

4.4. Extended Variant on Attention Maps

Although Gray-PE can partially capture relative distances, it faces significant challenges when the input sequence length is large or when the downstream task is highly sensitive to long-range dependencies. For instance, when the input sequence length reaches 10^2 , Gray-PE can only distinguish a limited range of relative distances. To address this issue, we propose an extension of Gray-PE, referred to as Log-PE. Specifically, we simulate Equation 7 by directly adding a pre-assigned relative position map, denoted as $\mathbf{R}_{i,j}$, to the attention map produced by the XNOR-based SSA operation. To be formal:

$$\mathbf{AttnMap} = \sum_{i=0}^D \neg(\mathbf{Q} \oplus \mathbf{K}) + \mathbf{R}_{i,j} \quad (14)$$

where

$$\mathbf{R}_{i,j} = [R_{i,j}] = \left\lceil \left\lceil \log_2 \left(\frac{L-1}{|i-j|} \right) \right\rceil \right\rceil. \quad (15)$$

Here, $\lceil \cdot \rceil$ denotes the round-up function, L is the sequence length, and i, j Figure 2 (c) shows an illustration of Log-PE, indicating that the farther relative distance, the smaller $R_{i,j}$. Since the original $\mathbf{AttnMap} \in \mathbb{N}_0$ is a matrix composed of non-negative integers, our primary goal is to ensure accurate relative distance consistency while preserving the effectiveness of spiking self-attention. If we set the $R_{i,j}$ as $\frac{L-1}{|i-j|}$, we could obtain a complete relative positional encoding for the XNOR-based SSA. However, we choose not to pursue this solution because, for long sequence lengths L , the large values of $\frac{L-1}{|i-j|}$ would severely distort the original representations in the spiking self-attention map. Therefore, using the logarithmic form $R_{i,j}$ represents a trade-off

that balances the values of the attention map and relative positional encoding.

4.5. Two-Dimensional Form for Image Patches

CNN-based SNN models, such as Spiking VGG (Sengupta et al., 2019) and SEW-ResNet (Fang et al., 2021), do not incorporate the concept of ‘‘positional encoding’’ in their spike representations. In contrast, Vision Transformer (Dosovitskiy et al., 2021) reformulated traditional image classification into a patch-based approach, dividing images into smaller patches. Unlike 1D positional encoding, which only considers the linear sequence of patches, 2D RPE accounts for **both the horizontal and vertical** positions of the patches in the image grid. This ensures that the model can recognize the relative positions along a single axis and the crucial interactions between patches across both dimensions. In our implementation, we assign horizontal and vertical positions with independent dimensions to store the Gray Code. Formally, the attention map **AttnMap** is:

$$\mathbf{AttnMap} = \sum_{i=0}^D \neg([\mathbf{Q} \parallel G(\mathbf{h}) \parallel G(\mathbf{w})] \oplus [\mathbf{K} \parallel G(\mathbf{h}) \parallel G(\mathbf{w})]). \quad (16)$$

Here, \mathbf{h} is the array of position indexes, specifically $\mathbf{h} = [0, 1, 2, \dots, h-1]$, where h denotes the maximum patch index along the height axis. Similarly, \mathbf{w} is along the width axis. We show our 2D form in Figure 2 (d).

5. Experiments

5.1. Datasets

To evaluate the RPE capabilities of the compared models, we conduct experiments on two sequential tasks: **time-series forecasting** and **text classification**. Following Lv et al. (2024b), we choose 4 real-world datasets for time-series forecasting: Metr-la (Li et al., 2017b), Pems-bay (Li et al., 2017b), Electricity (Lai et al., 2018), Solar (Lai et al., 2018). For text classification, we follow Lv et al. (2024a) and conduct experiments on six benchmark datasets: Movie Reviews (Pang & Lee, 2005), SST-2 (Socher et al., 2013), SST-5, Subj, ChnSenti, and Waimai. Additionally, to demonstrate the versatility of our RPE method in image processing, we perform **patch-based image classification** experiments on one static dataset, CIFAR, and one neuromorphic dataset, CIFAR10-DVS (Li et al., 2017a). The details of these datasets, metrics, and training hyper-parameters are provided in Appendix B.

5.2. Time-Series Forecasting

Time-series forecasting is a suitable task for evaluating the effectiveness of our proposed RPE method because it involves capturing the temporal dependencies between data

Table 1. Experimental results of time-series forecasting on 4 benchmarks with various prediction lengths 6, 24, 48, 96. “PE” stands for positional encoding. “R” denotes relative PE, while “A” denotes absolute PE. “w/o” denotes “without” while “w/” denotes “with”. The best results for each series of SNNs are highlighted in bold font. \uparrow (indicating "higher is better") and \downarrow (indicating "lower is better") are used to denote performance metrics. Results highlighted with shading are ours. All results are averaged across 3 random seeds.

Models	PE		Metric	Metr-la (Short)				Pems-bay (Short)				Solar (Long)				Electricity (Long)				Avg.
	Spike	Type		6	24	48	96	6	24	48	96	6	24	48	96	6	24	48	96	
Transformer w/ RPE	\times	R	R \uparrow	.729	.560	.416	.306	.787	.730	.694	.676	.951	.854	.763	.720	.984	.978	.974	.968	.756
			RSE \downarrow	.548	.696	.802	.878	.499	.563	.600	.617	.225	.373	.492	.539	.251	.274	.341	.420	.507
Transformer w/ Sin-PE	\times	A	R \uparrow	.727	.554	.413	.284	.785	.734	.688	.673	.953	.858	.759	.718	.978	.975	.972	.964	.752
			RSE \downarrow	.551	.704	.808	.895	.502	.558	.610	.618	.223	.377	.504	.545	.260	.277	.347	.425	.512
Spikformer w/o PE	-	-	R \uparrow	.697	.491	.383	.242	.768	.684	.678	.663	.903	.819	.715	.656	.956	.955	.953	.943	.719
			RSE \downarrow	.581	.753	.828	.917	.521	.607	.613	.627	.319	.439	.548	.602	.371	.375	.386	.450	.559
Spikformer w/ Conv-PE (Original)	\checkmark	A	R \uparrow	.713	.527	.399	.267	.773	.697	.686	.667	.929	.828	.744	.674	.959	.955	.955	.954	.733
			RSE \downarrow	.565	.725	.818	.903	.514	.594	.606	.621	.272	.426	.519	.586	.373	.371	.379	.382	.541
Spikformer w/ CPG-PE	\checkmark	A	R \uparrow	.726	.526	.419	.287	.780	.712	.690	.666	.937	.833	.757	.707	.972	.970	.966	.960	.744
			RSE \downarrow	.553	.720	.806	.890	.508	.580	.602	.622	.257	.420	.506	.555	.299	.310	.314	.355	.519
Spikformer-XNOR w/o PE	-	-	R \uparrow	.699	.488	.380	.244	.764	.680	.679	.666	.906	.820	.721	.653	.960	.958	.951	.943	.720
			RSE \downarrow	.575	.758	.830	.914	.525	.614	.613	.621	.315	.438	.540	.608	.364	.373	.390	.455	.558
Spikformer-XNOR w/ Conv-PE	\checkmark	A	R \uparrow	.718	.531	.405	.269	.771	.693	.690	.665	.928	.829	.740	.669	.960	.957	.955	.953	.733
			RSE \downarrow	.559	.721	.813	.910	.518	.599	.613	.628	.273	.421	.527	.595	.365	.371	.376	.384	.542
Spikformer-XNOR w/ Binary-PE	\checkmark	-	R \uparrow	.701	.488	.384	.252	.759	.698	.675	.644	.918	.815	.707	.677	.964	.959	.949	.945	.721
			RSE \downarrow	.575	.754	.827	.911	.531	.593	.616	.645	.293	.441	.555	.594	.334	.357	.402	.448	.555
Spikformer-XNOR w/ Gray-PE	\checkmark	R	R \uparrow	.728	.544	.414	.295	.782	.724	.694	.673	.936	.840	.756	.710	.974	.972	.966	.962	.748
			RSE \downarrow	.546	.706	.806	.885	.506	.578	.597	.618	.257	.409	.507	.546	.276	.304	.320	.342	.513
Spikformer-XNOR w/ Log-PE	\checkmark	R	R \uparrow	.735	.535	.424	.290	.789	.717	.691	.670	.933	.841	.758	.734	.978	.974	.968	.964	.750
			RSE \downarrow	.543	.719	.799	.876	.496	.575	.601	.620	.265	.408	.504	.525	.272	.300	.314	.340	.509
QKFormer w/o PE (Original)	-	-	R \uparrow	.702	.501	.377	.240	.750	.702	.664	.655	.905	.751	.497	.375	.964	.963	.958	.955	.685
			RSE \downarrow	.578	.740	.830	.924	.542	.595	.634	.633	.316	.513	.746	.812	.350	.352	.368	.371	.582
QKFormer w/ Conv-PE	\checkmark	A	R \uparrow	.717	.513	.376	.246	.767	.706	.681	.654	.920	.748	.512	.416	.970	.967	.963	.958	.695
			RSE \downarrow	.561	.735	.832	.917	.521	.586	.609	.635	.289	.515	.716	.784	.306	.319	.355	.367	.565
QKFormer w/ CPG-PE	\checkmark	A	R \uparrow	.740	.554	.419	.276	.783	.714	.702	.660	.922	.754	.702	.604	.977	.969	.968	.963	.732
			RSE \downarrow	.536	.704	.803	.896	.503	.578	.589	.633	.285	.520	.581	.645	.266	.312	.315	.332	.531
QKFormer-XNOR w/ Gray-PE	\checkmark	R	R \uparrow	.742	.551	.418	.274	.799	.715	.691	.674	.927	.817	.710	.691	.974	.970	.968	.965	.742
			RSE \downarrow	.534	.711	.804	.898	.484	.577	.601	.616	.276	.438	.556	.570	.277	.310	.314	.331	.519
QKFormer-XNOR w/ Log-PE	\checkmark	R	R \uparrow	.742	.541	.416	.265	.801	.710	.707	.661	.928	.818	.748	.698	.978	.974	.972	.966	.746
			RSE \downarrow	.535	.715	.805	.903	.482	.581	.585	.629	.274	.437	.515	.564	.264	.285	.296	.328	.514

points over time. We follow the framework outlined by Lv et al. (2024b) to conduct time-series forecasting experiments using SNN models. Specifically, we use Spikformer (Zhou et al., 2023b) and the current state-of-the-art (SOTA) model, QKFormer (Zhou et al., 2024), as the backbone architectures, both of which incorporate spiking self-attention mechanisms. We modify the spiking self-attention mechanism as outlined in Section 4.2 to create two variants: Spikformer-XNOR and QKFormer-XNOR. Subsequently, we integrate our proposed Gray-PE and its extended forms into these SNN architectures.

For the baseline comparisons, we consider the following: (1) spiking absolute PE and CPG-PE (Lv et al., 2024a), (2) the PE used in the original architectures, referred to as Conv-PE, and (3) the integration of Binary-PE into the XNOR-based SSA. To isolate the effects of the XNOR modification, we also perform experiments on Spikformer-XNOR and QKFormer-XNOR without any positional encoding, as well as with Conv-PE. We present the performance of the compared SNN models with various positional encoding methods in Table 1. The key findings are as follows:

(1) Relative PE generally outperforms absolute PE in time-series forecasting tasks. Based on the comparison between the Transformer with RPE and sinusoidal-PE, as well as Spikformer-XNOR with Conv-PE and Gray-PE, we observe that relative PE consistently outperforms absolute PE, particularly on long-term time-series datasets such as

Solar and Electricity.

(2) The XNOR modification does not impact the performance of the original SNN models. The average performance of Spikformer without PE is nearly identical to that of Spikformer-XNOR without PE. This suggests that our XNOR modification of the SSA does not affect the performance of the original SNN models. Consequently, we can attribute the observed performance improvements solely to the introduced positional encoding techniques, excluding any impact from the XNOR operation itself.

(3) Gray-PE and its extended form, Log-PE, enable Spikformer and QKFormer to achieve the best performance among their variants. CPG-PE is a spiking version of absolute PE designed for SNNs. Spikformer and QKFormer, when equipped with our proposed Gray-PE and Log-PE, consistently outperform all other corresponding variants, including CPG-PE and Binary-PE. Furthermore, we were surprised to find that Binary-PE fails to capture the relative positional information. This leads us to reconsider the underlying issue: if a binary encoding method cannot represent distances between certain positions, it is unsuitable as an RPE solution for SNNs. In contrast, Gray Code and Log-PE provide approximate binary encoding approaches that “partially” achieve this goal.

(4) For long input sequences, Log-PE is more effective than Gray-PE in capturing relative positional information. The input sequence length for Metr-la and Pems-bay

Table 2. Accuracy (%) on 6 text classification benchmarks. The best results of SNNs and ANNs are formatted in bold font. We set the sentence length to 128 for the English dataset and 32 for the Chinese dataset. Experimental results are averaged across 5 random seeds.

Model	PE		Param (M)	English Dataset (Length = 128)				Chinese Dataset (Length = 32)		Avg.
	Spike	Type		MR	SST-2	Subj	SST-5	ChnSenti	Waimai	
Fine-tuned BERT	X	A	109.8	87.63 ±0.18	92.31 ±0.17	95.90 ±0.16	50.41 ±0.13	89.48 ±0.16	90.27 ±0.13	84.33
Spikformer w/o PE	-	-	109.8	75.87±0.35	81.71±0.31	91.60±0.30	41.84±0.39	85.62±0.25	86.87±0.28	77.25
Spikformer w/ CPG-PE	✓	A	110.4	82.42±0.42	82.90±0.33	92.50±0.25	43.62±0.36	86.54±0.26	88.49 ±0.29	79.41
Spikformer-XNOR w/o PE	-	-	109.8	75.80±0.40	81.74±0.40	91.50±0.29	41.88±0.38	85.64±0.31	86.66±0.33	77.20
Spikformer-XNOR w/ Gray-PE	✓	R	109.8	83.73±0.45	84.52±0.39	92.50±0.33	44.06±0.48	87.41±0.36	88.40±0.30	80.11
Spikformer-XNOR w/ Log-PE	✓	R	109.8	83.88 ±0.40	84.64 ±0.37	92.80 ±0.30	44.52 ±0.43	87.95 ±0.34	88.46±0.28	80.38

is 12, whereas, for Solar and Electricity, it is 168. As an approximated approach of RPE, Gray-PE can only represent the distance between two indexes differing by 2^n . This limitation means that SNNs using Gray-PE may experience a performance drop when processing longer input sequences. Furthermore, on the long-sequence datasets Solar and Electricity, SNNs equipped with Log-PE consistently outperform those with Gray-PE across nearly all prediction length settings. For instance, on the Solar dataset with a prediction length of 48, QKFormer with Log-PE significantly outperforms QKFormer with Gray-PE, showing an average improvement of 0.038 in R^2 . This result indicates that Log-PE is more effective for processing long input sequences.

5.3. Text Classification

Text classification is another representative task for which RPE plays an important role. Therefore, we conduct experiments to evaluate the performance of SNNs with RPE in text classification tasks, comparing it against other PE techniques to highlight its advantages in capturing complex linguistic structures and contextual nuances. For this part, we strictly follow the experimental setup used in the text classification experiments in Lv et al. (2024a), and the results are presented in Table 2.

Based on the results in Table 2, it is evident that our proposed Gray-PE and Log-PE significantly outperform the other spiking positional encoding methods across several key benchmarks. Both Gray-PE and Log-PE demonstrate superior accuracy on the English and Chinese datasets, with particularly notable improvements on MR, SST-2, Subj, and ChnSenti. However, the performance of RPE on the Waimai dataset is not as strong as that of CPG-PE. We attribute this to the nature of the dataset, which consists of user reviews often containing informal language, typos, or mixed expressions. This noise can hinder the model’s ability to extract meaningful patterns. These results highlight the advantages of our proposed spiking RPE techniques, especially in handling the dependencies and varying word order in text classification tasks. Unlike spiking absolute PE, i.e., CPG-PE, which struggles to adapt to the nuances of language, Gray-PE and Log-PE provide a more flexible and context-sensitive representation, improving the model’s ability to classify sentences accurately.

5.4. Patch-based Image Classification

We also conduct experiments on ViT-based SNNs, including Spikformer and the current SOTA model, QKFormer. As discussed in Section 4.5, we extend Gray-PE into a **two-dimensional form** and integrate it into the patch-based framework to enhance the spatial relationship understanding of spiking Transformers. The results of these experiments are presented in Table 3, where we draw conclusions that:

(1) Gray-PE enhances the performance of Spikformer with less parameters. Gray-PE, whether in 1D or 2D form, consistently improves Spikformer’s classification accuracy. As an approximation of RPE, Gray-PE successfully outperforms spiking absolute PE (i.e., CPG-PE), highlighting the strong dependency between patches within an image. Notably, Spikformer-XNOR with Gray-PE 2D achieves the highest performance across all three datasets, demonstrating the effectiveness of 2D form Gray-PE in capturing relative positional information.

(2) On image classification, QKFormer is insensitive to positional encoding. Surprisingly, QKFormer shows limited improvements or even performance drops when using PE techniques. Whether with CPG-PE or Gray-PE, QKFormer fails to achieve significant performance gains and, in fact, shows a decline in performance. We attribute this phenomenon to the special attention mechanism in QKFormer, known as “q-k attention”, which sums the query matrix along the channel dimension before performing a dot product with key matrix. This strategy eliminates the positional representation provided by both CPG-PE and Gray-PE, which negatively impacts performance.

(3) For Gray-PE, the 2D form performs better than the 1D form on processing image patches. Through a comparison of the performance of SNNs using Gray-PE 1D and 2D, we find that the design of the two-dimensional form of Gray Code is effective. In the case of Spikformers, Gray-PE 2D significantly outperforms Gray-PE 1D, with a 0.44% accuracy improvement averagely. Even for QKFormer, where PE’s influence is limited, Gray-PE 2D still far outperforms its 1D variant. These results confirm that Gray-PE 2D is superior to Gray-PE 1D in handling positional information for image classification tasks, validating the success of our proposed Gray-PE 2D.

Table 3. Accuracy (%) on image classification benchmarks. Numbers with * denote our implementation, representing results that differ from those reported in the original papers. The best and second-best results are highlighted in bold and underlined formats, respectively. “R” denotes relative PE, while “A” denotes absolute PE. The results with shading are ours. Results are averaged across 4 random seeds.

Model	PE		CIFAR10		CIFAR10-DVS		CIFAR100		Avg.
	Spike	Type	Param (M)	Accuracy	Param (M)	Accuracy	Param (M)	Accuracy	
Vision-Transformer	X	A	9.32	96.73	–	–	9.36	81.02	–
Spikformer w/o PE	–	–	8.00	93.98	1.99	76.60	8.04	74.02	81.53
Spikformer w/ Conv-PE (Original)	✓	A	9.32	94.80*	2.57	78.10*	9.36	77.04*	83.31
Spikformer w/ CPG-PE	✓	A	8.17	95.06	2.06	<u>78.40</u>	8.20	77.82	83.76
Spikformer-XNOR w/o PE	–	–	8.00	94.14	1.99	76.70	8.04	74.16	81.67
Spikformer-XNOR w/ Conv-PE	✓	A	9.32	95.20	2.57	77.90	9.36	78.04	83.71
Spikformer-XNOR w/ Gray-PE 1D	✓	R	8.00	<u>95.46</u>	1.99	77.90	8.04	<u>78.12</u>	<u>83.83</u>
Spikformer-XNOR w/ Gray-PE 2D	✓	R	8.00	95.66	1.99	78.70	8.04	78.45	84.27
QKFormer w/o PE (Original)	–	–	6.74	<u>96.32</u> *	1.50	83.40 *	6.76	80.90 *	86.87
QKFormer w/ CPG-PE	✓	A	7.01	96.30	1.58	82.00	7.04	80.52	86.27
QKFormer-XNOR w/o PE	–	–	6.74	96.28	1.50	82.90	6.76	80.80	86.66
QKFormer-XNOR w/ Gray-PE 1D	✓	R	6.74	96.22	1.50	82.20	6.76	80.48	86.30
QKFormer-XNOR w/ Gray-PE 2D	✓	R	6.74	96.36	1.50	<u>83.10</u>	6.76	<u>80.82</u>	<u>86.76</u>

5.5. Positional Encoding Analysis

In this section, we will analyze the following points: (1) Impact of the number of bits on the performance of SNNs when using Gray-PE. (2) Rationale behind why we use an approximate RPE rather than a complete one in SNNs.

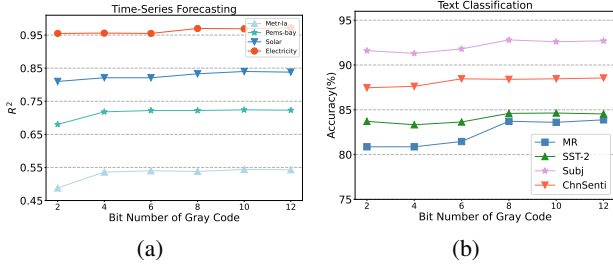


Figure 3. Spikformer-XNOR with Gray-PE across various bit numbers ranging from 2 to 12 on (a) time-series forecasting tasks and (b) text classification tasks.

For the first question, we present the results of our parameter sensitivity experiments in Figure 3. Consider that: if the number of bits used for encoding relative positions in Gray-PE is b , then the total number of unique encodings possible is 2^b . We set the maximum sequence length is L , so relative distances range from 1 to $L-1$. According to the pigeonhole principle, if $L-1 > 2^b$, there will inevitably be at least two distances that are represented identically. This issue can be mitigated by increasing b to cover the range of relative distances up to $L-1$. From Figure 3 (a), we observe that for long-sequence datasets, such as Solar and Electricity (Length = 168), the number of bits should be at least 7 to avoid Gray-PE missing relative positional information. However, for shorter datasets like Metr-la (Length = 12) and ChnSenti (Length = 32), 5 bits are sufficient.

Regarding the second question, we show the performance of SNNs using complete RPE (C-RPE). As discussed in Section 4.4, C-RPE is obtained by setting $R_{i,j}$ as $\frac{L-1}{|i-j|}$

Table 4. Time-series forecasting performance of SNNs trained with Complete RPE (C-RPE) method. We take Metr-la and Electricity as examples. * denotes failure to converge.

Model (Prediction Length = 24)	Metr-la ($L = 12$)		Electricity ($L = 168$)	
	$R^2 \uparrow$	RSE \downarrow	$R^2 \uparrow$	RSE \downarrow
Spikformer-XNOR w/o PE	.491	.753	.955	.375
Spikformer-XNOR w/ Log-PE	.535	.719	.974	.300
Spikformer-XNOR w/ C-RPE	.158*	.967*	.710*	1.03*
QKFormer-XNOR w/o PE	.501	.740	.963	.352
QKFormer-XNOR w/ Log-PE	.541	.715	.974	.285
QKFormer-XNOR w/ C-RPE	.430	.824	.710*	1.03*

and adding it to the attention map. However, the large values of this method can cause the vanilla attention map to fail in recording accurate similarity scores. As shown in Table 4, we observe that SNNs with C-RPE significantly underperform compared to other variants, with some even failing to converge, due to the detrimental impact of the large positional encoding values on the training process.

Besides, we design another extended form of Gray-PE, leveraging hierarchical relative positional representation. However, we find that when an encoding method involves carry-over, ensuring the uniqueness of the spike representation for each relative distance becomes challenging. A detailed analysis of this issue can be found in Appendix C.

6. Conclusion

In this paper, we propose a series of relative positional encoding methods for spiking Transformers. Our approach preserves the spiking nature of SNNs while effectively representing relative distances. Experimental evaluations on time series forecasting, text classification, and image classification demonstrate significant performance improvements. These results validate the effectiveness of the proposed RPE method and highlight its potential to enhance the versatility and applicability of SNNs across various domains. Future work and limitations are discussed in Appendix D.

Impact Statement

This research enhances spiking neural networks by introducing an approximation method for relative positional encoding method based on Gray Code. The proposed approach broadens the applicability of SNNs across diverse domains, enabling more robust and versatile neural architectures. Lastly, we do not think our work will negatively impact ethical aspects or future societal consequences.

References

- Dosovitskiy, A., Beyer, L., Kolesnikov, A., Weissenborn, D., Zhai, X., Unterthiner, T., Dehghani, M., Minderer, M., Heigold, G., Gelly, S., Uszkoreit, J., and Houslyby, N. An image is worth 16x16 words: Transformers for image recognition at scale. In *International Conference on Learning Representations*, 2021.
- Fang, W., Yu, Z., Chen, Y., Huang, T., Masquelier, T., and Tian, Y. Deep residual learning in spiking neural networks. In *Neural Information Processing Systems*, 2021.
- Gray, F. Pulse code communication. *United States Patent Number 2632058*, 1953.
- Hao, Y., Zhou, D., Wang, Z., Ngo, C.-W., and Wang, M. Posmlp-video: spatial and temporal relative position encoding for efficient video recognition. *International Journal of Computer Vision*, 132(12):5820–5840, 2024.
- Kingma, D. P. and Ba, J. Adam: A method for stochastic optimization. *arXiv preprint arXiv:1412.6980*, 2014.
- Lai, G., Chang, W.-C., Yang, Y., and Liu, H. Modeling long- and short-term temporal patterns with deep neural networks. In *The 41st International ACM SIGIR Conference on Research & Development in Information Retrieval*, pp. 95–104, 2018.
- Li, H., Liu, H., Ji, X., Li, G., and Shi, L. Cifar10-dvs: An event-stream dataset for object classification. *Frontiers in Neuroscience*, 11, 2017a.
- Li, Y., Yu, R., Shahabi, C., and Liu, Y. Diffusion convolutional recurrent neural network: Data-driven traffic forecasting. *arXiv preprint arXiv:1707.01926*, 2017b.
- Liao, Z., Liu, Y., Zheng, Q., and Pan, G. Spiking nerf: Representing the real-world geometry by a discontinuous representation. In *Proceedings of the AAAI Conference on Artificial Intelligence*, volume 38, pp. 13790–13798, 2024.
- Liu, Z., Lin, Y., Cao, Y., Hu, H., Wei, Y., Zhang, Z., Lin, S., and Guo, B. Swin transformer: Hierarchical vision transformer using shifted windows. In *Proceedings of the IEEE/CVF international conference on computer vision*, pp. 10012–10022, 2021.
- Loshchilov, I. and Hutter, F. Decoupled weight decay regularization. In *International Conference on Learning Representations*, 2018.
- Luo, X., Yao, M., Chou, Y., Xu, B., and Li, G. Integer-valued training and spike-driven inference spiking neural network for high-performance and energy-efficient object detection. In *European Conference on Computer Vision*, pp. 253–272. Springer, 2024.
- Lv, C., Li, T., Xu, J., Gu, C., Ling, Z., Zhang, C., Zheng, X., and Huang, X. Spikebert: A language spikformer learned from bert with knowledge distillation. 2023a.
- Lv, C., Xu, J., and Zheng, X. Spiking convolutional neural networks for text classification. In *The Eleventh International Conference on Learning Representations (ICLR)*, 2023b.
- Lv, C., Han, D., Wang, Y., Zheng, X., Huang, X., and Li, D. Advancing spiking neural networks for sequential modeling with central pattern generators. In *The Thirty-eighth Annual Conference on Neural Information Processing Systems*, 2024a.
- Lv, C., Wang, Y., Han, D., Zheng, X., Huang, X., and Li, D. Efficient and effective time-series forecasting with spiking neural networks. In *Forty-first International Conference on Machine Learning (ICML)*, 2024b.
- Maass, W. Networks of spiking neurons: the third generation of neural network models. *Neural Networks*, 14: 1659–1671, 1997.
- Marder, E. and Bucher, D. Central pattern generators and the control of rhythmic movements. *Current biology*, 11 (23):R986–R996, 2001.
- Pang, B. and Lee, L. Seeing stars: Exploiting class relationships for sentiment categorization with respect to rating scales. In *ACL*, 2005.
- Park, J.-h., Kim, D., Lee, J.-W., and Lee, E.-K. Poster: Hybrid encoding in snn-based transformers for accurate time series forecasting. In *2024 IEEE 21st International Conference on Mobile Ad-Hoc and Smart Systems (MASS)*, pp. 492–493. IEEE, 2024.
- Sengupta, A., Ye, Y., Wang, R., Liu, C., and Roy, K. Going deeper in spiking neural networks: Vgg and residual architectures. *Frontiers in neuroscience*, 13:95, 2019.
- Socher, R., Perelygin, A., Wu, J., Chuang, J., Manning, C. D., Ng, A., and Potts, C. Recursive deep models for semantic compositionality over a sentiment treebank. In *EMNLP*, 2013.

- Su, J., Ahmed, M., Lu, Y., Pan, S., Bo, W., and Liu, Y. Roformer: Enhanced transformer with rotary position embedding. *Neurocomputing*, 568:127063, 2024.
- Vaswani, A. Attention is all you need. *Advances in Neural Information Processing Systems*, 2017.
- Xing, X., Zhang, Z., Ni, Z., Xiao, S., Ju, Y., Wang, Y., Zhang, J., Li, G., et al. Spikelm: Towards general spike-driven language modeling via elastic bi-spiking mechanisms. In *Forty-first International Conference on Machine Learning*, 2024.
- Yao, M., Hu, J., Zhou, Z., Yuan, L., Tian, Y., Bo, X., and Li, G. Spike-driven transformer. In *Thirty-seventh Conference on Neural Information Processing Systems*, 2023.
- Yao, M., Hu, J., Hu, T., Xu, Y., Zhou, Z., Tian, Y., XU, B., and Li, G. Spike-driven transformer v2: Meta spiking neural network architecture inspiring the design of next-generation neuromorphic chips. In *The Twelfth International Conference on Learning Representations*, 2024a.
- Yao, M., Qiu, X., Hu, T., Hu, J., Chou, Y., Tian, K., Liao, J., Leng, L., Xu, B., and Li, G. Scaling spike-driven transformer with efficient spike firing approximation training. *arXiv preprint arXiv:2411.16061*, 2024b.
- Zhou, C., Yu, L., Zhou, Z., Zhang, H., Ma, Z., Zhou, H., and Tian, Y. Spikingformer: Spike-driven residual learning for transformer-based spiking neural network. *arXiv preprint arXiv:2304.11954*, 2023a.
- Zhou, C., Zhang, H., Zhou, Z., Yu, L., Huang, L., Fan, X., Yuan, L., Ma, Z., Zhou, H., and Tian, Y. Qkformer: Hierarchical spiking transformer using q-k attention. In *The Thirty-eighth Annual Conference on Neural Information Processing Systems*, 2024.
- Zhou, Z., Zhu, Y., He, C., Wang, Y., Yan, S., Tian, Y., and Yuan, L. Spikformer: When spiking neural network meets transformer. In *The Eleventh International Conference on Learning Representations, ICLR 2023, Kigali, Rwanda, May 1-5, 2023*, 2023b.
- Zhu, R.-J., Zhao, Q., and Eshraghian, J. K. Spikegpt: Generative pre-trained language model with spiking neural networks. *arXiv preprint arXiv:2302.13939*, 2023.

A. Proof of Theorem 4.1

This section provides a detailed mathematical proof of Theorem 4.1.

A.1. Statement

For any non-negative integer n , and for any pair of integers a and $b = a + 2^n$, the Hamming distance between their Gray Code representations $G(a)$ and $G(b)$ is:

$$d_H(G(a), G(b)) = \begin{cases} 1 & \text{if } n = 0, \\ 2 & \text{if } n \geq 1. \end{cases} \quad (17)$$

A.2. Proof

We aim to determine the Hamming distance $d_H(G(a), G(a + 2^n))$.

A.2.1. CASE 1: $n = 0$

When $n = 0$, $b = a + 1$. By the definition of the Gray Code:

$$G(a) = a \oplus (a \gg 1), \quad G(a + 1) = (a + 1) \oplus ((a + 1) \gg 1). \quad (18)$$

The Gray Code inherently ensures that consecutive integers differ by exactly one bit. Therefore:

$$d_H(G(a), G(a + 1)) = 1. \quad (19)$$

This establishes the base case for $n = 0$.

A.2.2. CASE 2: $n \geq 1$

For $n \geq 1$, consider $b = a + 2^n$. We analyze the XOR of their Gray Codes:

$$\begin{aligned} & G(a) \oplus G(a + 2^n) \\ &= (a \oplus (a \gg 1)) \oplus ((a + 2^n) \oplus ((a + 2^n) \gg 1)). \end{aligned} \quad (20)$$

Rearranging the terms:

$$\begin{aligned} & G(a) \oplus G(a + 2^n) \\ &= (a \oplus (a + 2^n)) \oplus ((a \gg 1) \oplus ((a + 2^n) \gg 1)). \end{aligned} \quad (21)$$

Analyzing $a \oplus (a + 2^n)$: Adding 2^n to a flips the n -th bit of a . Therefore:

$$a \oplus (a + 2^n) = 2^n. \quad (22)$$

Analyzing $(a \gg 1) \oplus ((a + 2^n) \gg 1)$: Shifting both a and $a + 2^n$ to the right by one bit:

$$(a + 2^n) \gg 1 = (a \gg 1) + 2^{n-1}. \quad (23)$$

Thus:

$$\begin{aligned} & (a \gg 1) \oplus ((a + 2^n) \gg 1) \\ &= (a \gg 1) \oplus ((a \gg 1) + 2^{n-1}) \\ &= 2^{n-1}. \end{aligned} \quad (24)$$

Combining the Results:

$$G(a) \oplus G(a + 2^n) = 2^n \oplus 2^{n-1}. \quad (25)$$

In binary representation, 2^n and 2^{n-1} have single 1's in distinct positions. Their XOR results in a binary number with exactly two 1's:

$$2^n \oplus 2^{n-1} = 2^n + 2^{n-1}. \quad (26)$$

Therefore, the Hamming weight (number of 1's) of $G(a) \oplus G(a + 2^n)$ is 2.

Therefore, for $n \geq 1$, since the XOR of the Gray Codes yields a binary number with exactly two 1's, the Hamming distance between $G(a)$ and $G(a + 2^n)$ is:

$$d_H(G(a), G(a + 2^n)) = 2. \tag{27}$$

A.3. Final Conclusion

Combining both cases, we conclude that for any non-negative integer n :

$$d_H(G(a), G(a + 2^n)) = \begin{cases} 1 & \text{if } n = 0, \\ 2 & \text{if } n \geq 1. \end{cases} \tag{28}$$

This rigorously proves the observed property of Gray Codes concerning the Hamming distance between numbers differing by powers of two.

B. Experimental Settings

B.1. Datasets

B.1.1. TIME-SERIES FORECASTING

We strictly follow the dataset settings of CPG-PE (Lv et al., 2024a). The datasets we used are as follows: Metr-la (Li et al., 2017b): Average traffic speed data collected from highways in Los Angeles County. Pems-bay (Li et al., 2017b): Average traffic speed data from the Bay Area. Electricity (Lai et al., 2018): Hourly electricity consumption data in kilowatt-hours (kWh) of 321 clients. Solar (Lai et al., 2018): Solar power production. The detailed statistical characteristics and distribution ratios for each dataset are presented below:

Table 5. The statistics of time-series datasets.

Dataset	Samples	Variables	Observation Length	Train-Valid-Test Ratio
Metr-la	34, 272	207	12, (short-term)	(0.7, 0.2, 0.1)
Pems-bay	52, 116	325	12, (short-term)	(0.7, 0.2, 0.1)
Solar-energy	52, 560	137	168, (long-term)	(0.6, 0.2, 0.2)
Electricity	26, 304	321	168, (long-term)	(0.6, 0.2, 0.2)

B.1.2. TEXT CLASSIFICATION

For text classification, we follow Lv et al. (2023b) to conduct experiments on six easy discrimination tasks, covering both English and Chinese datasets. Here are the datasets we used in text classification experiments:

The MR dataset, which stands for Movie Review, contains movie-review documents labeled based on their overall sentiment polarity (positive or negative) or subjective rating (Pang & Lee, 2005).

SST-5 includes 11, 855 sentences from movie reviews for sentiment classification across five categories: very negative, negative, neutral, positive, and very positive (Socher et al., 2013).

SST-2 is the binary version of SST-5, containing only two classes: positive and negative. The Subj dataset is designed to classify sentences as either subjective or objective¹.

ChnSenti consists of approximately 7, 000 Chinese hotel reviews, each annotated with a positive or negative label².

Waimai contains around 12,000 Chinese user reviews from a food delivery platform, intended for binary sentiment classification (positive and negative)³.

¹<https://www.cs.cornell.edu/people/pabo/movie-review-data/>

²https://raw.githubusercontent.com/SophonPlus/ChineseNlpCorpus/master/datasets/ChnSentiCorp_htl_all/ChnSentiCorp_htl_all.csv

³https://raw.githubusercontent.com/SophonPlus/ChineseNlpCorpus/master/datasets/waimai_10k/waimai_10k.csv

B.1.3. IMAGE CLASSIFICATION

Here are the datasets we used in image classification experiments:

The CIFAR dataset is one of the most widely used benchmarks for image classification, comprising a collection of 60,000 color images, each with a resolution of 32×32 pixels. These images are partitioned into 50,000 training samples and 10,000 test samples. The dataset includes 10 classes, each containing 6,000 images, and spans a variety of object categories such as airplanes, cars, birds, and cats. The relatively low resolution of the images makes the dataset a challenging benchmark for evaluating model performance in small-scale image classification tasks.

The CIFAR10-DVS dataset represents a neuromorphic adaptation of the original CIFAR10 set, where static images have been converted into dynamic representations that simulate the recording capabilities of a Dynamic Vision Sensor (DVS) camera. Unlike traditional cameras, a DVS captures changes in the scene as individual events, rather than capturing full-frame images at fixed time intervals. This conversion results in a dataset that is more aligned with how biological vision systems process information. The CIFAR10-DVS dataset consists of 9,000 training samples and 1,000 test samples, with a higher resolution of 128×128 pixels compared to the original CIFAR10. The event-driven nature of this dataset presents unique challenges in terms of processing and model adaptation, as it requires handling sparse, asynchronous event streams rather than dense, synchronous pixel data. This dataset is particularly valuable for testing models designed for neuromorphic systems and event-based vision tasks, offering a more realistic and biologically plausible approach to image classification.

B.2. Time-series Forecasting

Metrics The metrics we used in time-series forecasting are the coefficient of determination (R^2) and the Root Relative Squared Error (RSE).

$$R^2 = \frac{1}{MCL} \sum_{m=1}^M \sum_{c=1}^C \sum_{l=1}^L \left[1 - \frac{(Y_{c,l}^m - \hat{Y}_{c,l}^m)^2}{(Y_{c,l}^m - \bar{Y}_{c,l})^2} \right], \quad (29)$$

$$\text{RSE} = \sqrt{\frac{\sum_{m=1}^M \|\mathbf{Y}^m - \hat{\mathbf{Y}}^m\|^2}{\sum_{m=1}^M \|\mathbf{Y}^m - \bar{\mathbf{Y}}\|^2}}. \quad (30)$$

In these formulas, M represents the size of the test set, C denotes the number of channels, and L signifies the length of the predictions. $\bar{\mathbf{Y}}$ is the average of \mathbf{Y}^m . The term $Y_{c,l}^m$ refers to the l -th future value of the c -th variable for the m -th sample, while $\bar{Y}_{c,l}$ represents the mean of $Y_{c,l}^m$ across all samples. The symbols $\hat{\mathbf{Y}}^m$ and $\hat{Y}_{c,l}^m$ are used to denote the predicted values. Compared to Mean Squared Error (MSE) or Mean Absolute Error (MAE), these metrics exhibit greater resilience to the absolute values of the datasets, making them especially valuable in time-series forecasting tasks.

Model Architecture All SNNs take 4 time steps for spiking neurons. We construct all Spikformer as 2 blocks, setting the feature dimension as 256, and the hidden feature dimension in FFN as 1024. As for QKFormer, we set the block number as 4, 2 of which are QK blocks and the other 2 are Spikformer blocks.

Training Hyper-parameters we set the training batch size as 32 and adopt Adam (Kingma & Ba, 2014) optimizer with a cosine scheduler of learning rate 1×10^{-4} . An early stopping strategy with a tolerance of 30 epochs is adopted. For other configurations, we honestly follow the SeqSNN framework⁴ proposed by Lv et al. (2024b). We conducted time-series forecasting experiments on 24G-V100 GPUs. On average, a single experiment takes about 1 hour under the settings above.

B.3. Text Classification

Model Achitecture All Spikformers are with 12 encoder blocks and 768 feature embedding dimension. We have substituted layer normalization of SpikeBERT (Lv et al., 2023a) with batch normalization in our directly-trained Spikformer models for text classification tasks.

Training Hyper-parameters We directly trained Spikformers with arctangent surrogate gradients on all datasets. We use the BERT-TOKENIZER in Huggingface⁵ to tokenize the sentences to token sequences. We pad all samples to the same

⁴<https://github.com/microsoft/SeqSNN>

⁵<https://huggingface.co/>

sequence length of 256. We conducted text classification experiments on 4 RTX-3090 GPUs, and set the batch size as 32, optimizer as AdamW (Loshchilov & Hutter, 2018) with weight decay of 5×10^{-3} , and set a cosine scheduler of starting learning rate of 5×10^{-4} . What’s more, in order to speed up the training stage, we adopt the automatic mixed precision training strategy. On average, a single experiment takes about 1.5 hours under the settings above.

B.4. Image Classification

Model Architecture For all Spikformer models, we standardized the configuration to include 4 time steps. Specifically, for the CIFAR10 and CIFAR100 datasets, the models were uniformized with 4 encoder blocks and a feature embedding dimension of 384. For the CIFAR10-DVS dataset, the models were adjusted to have 2 encoder blocks and a feature embedding dimension of 256. For all QKFormers, we set the block number as 4, where 2 blocks are QK blocks and the other 2 are Spikformer blocks.

Training Hyper-parameters We honestly follow the experimental settings in Spikformer (Zhou et al., 2023b) and QKFormer (Zhou et al., 2024), whose source code and configuration files are available at <https://github.com/ZK-Zhou/spikformer> and <https://github.com/zhouchenlin2096/QKFormer>. As the training epochs are quite big (300 or 400 epochs) in their settings, we choose to use one 80G-A100 GPU, and it takes about 3 hours to conduct a single experiment, on average.

C. Analysis on Carry-Over

We observe that when the encoding method involves **carry-over**, as in binary systems, it becomes difficult to ensure the uniqueness of the spike representation for each relative distance, especially with limited dimensions in the query and key vectors during self-attention. The carry-over operation introduces dependencies between bits, meaning the encoding of one bit can influence the encoding of higher-order bits. Consequently, the Hamming distance between the encodings of different relative distances is not fixed and can vary significantly due to carry-over. These dependencies also increase the likelihood of encoding collisions, where different relative distances might share identical or similar binary encodings. This can be empirically demonstrated by the poor performance of SNNs with Binary-PE in time-series forecasting, as shown in Table 1. From this perspective, Gray-PE and its extended variants can be viewed as approximate solutions, as they **partially address** the challenge of ensuring unique spike representations for a range of relative distances.

D. Limitations and Future Work

D.1. Limitations

Despite the promising enhancements introduced by our Gray Code-based relative positional encoding method for spiking neural networks, several limitations must be acknowledged. Firstly, the current Gray Code implementation may encounter scalability issues when applied to very long input sequences or more complex network architectures. Additionally, while Gray Code effectively preserves binary spike representations, it may limit the flexibility and adaptability of the encoding scheme across diverse data modalities and task requirements. Furthermore, our evaluations have been confined to specific applications such as time series forecasting, text classification, and image patch classification, which may not fully capture the method’s performance in other domains, such as object detection (Luo et al., 2024) and real-world geometry representation (Liao et al., 2024).

D.2. Future Work

Future work should focus on optimizing the Gray Code-based RPE to enhance its scalability and efficiency, enabling its deployment in larger and more intricate SNN models. Exploring alternative encoding strategies or hybrid approaches could provide greater flexibility and improve the robustness of positional encoding across various data types and tasks. Expanding the scope of evaluation to include a wider range of applications would offer a more comprehensive understanding of the method’s effectiveness. Additionally, integrating Gray Code-based RPE with other advanced neural network components, such as attention mechanisms or neuromorphic hardware, could further elevate the performance and practical utility of SNNs. These efforts will contribute to the advancement of more versatile and powerful biologically inspired neural network architectures.